Radar interferometric phase errors induced by Faraday rotation[*]

Simon Zwieback and Franz J Meyer

October 28, 2020

Abstract

Ionospheric Faraday rotation distorts satellite radar observations of the Earth's surface. While its impact on radiometric observables is well understood, the errors in repeat-pass interferometric observables and hence in geodetic deformation analysis are largely unknown. Because the Faraday-induced errors cannot rigorously be compensated for in non-quadpol systems, it is imperative to determine their magnitude and nature. Focusing on distributed targets at L-band, we combine theoretical and empirical analyses for a range of land covers using airborne observations with simulated Faraday rotation.

We find that the typical deformation error is up to 2 mm in the co-pol channels but may exceed 5 mm for intense solar maxima. The cross-pol channel is more susceptible to severe errors. We identify the leakage of polarimetric phase contributions into the interferometric phase as a dominant error source. The polarimetric scattering characteristics induce a systematic dependence of the Faraday-induced deformation errors on land cover and topography. Also their temporal characteristics, with pronounced seasonal and quasi-decadal variability, predispose these systematic errors to be misinterpreted as deformation. While the relatively small magnitude of 1–2 mm is of limited concern in many applications, the persistence on semi- to multi-annual time scales compels attention when long-term deformation is to be estimated with millimetric accuracy. Phase errors induced by uncompensated Faraday rotation constitute an important and hitherto neglected error in interferometric deformation measurements.

1 Introduction

Microwaves propagating through the ionosphere are subject to Faraday rotation, which manifests as a rotation χ of the polarization plane of linearly polarized waves Wright et al. [2003], Meyer and Nicoll [2008]. Equivalently, the Earth's magnetic field turns the ionospheric plasma into a circularly birefringent medium [Appleton and Builder, 1933, Hartmann and Leitinger, 1984]. Left- and right-circularly-polarized waves propagate at slightly different phase velocities. The Faraday effect's magnitude increases with the total electron content (TEC) in the ionosphere in a way that also depends on the angle between the propagation direction and the Earth's magnetic field, and on the radar frequency Appleton and Builder [1933], Jokipii and Lerche [1969]. Spaceborne observations at lower frequencies are affected most significantly, with one-way Faraday angles χ of up to $30°$ at L-band [Freeman and Saatchi, 2004].

There is insufficient information in single- or dual-pol data to rigorously correct for Faraday rotation. This is in contrast to quad-pol observations, for which numerous physically based correction approaches have been devised [Wright et al., 2003, Meyer and Nicoll, 2008]. In analyses dealing with single- or dual-pol observations, usually no attempt is made to correct for Faraday rotation.

Uncompensated Faraday rotation distorts interferometric observations, as well as those of backscatter magnitudes and polarimetric parameters [Freeman and Saatchi, 2004, Schneider and Papathanassiou, 2007]. While these latter have been studied in detail, the Faraday-induced errors in interferometric analyses of distributed targets have received scant scrutiny. Reductions in the interferometric coherence due to Faraday rotation have been reported, their magnitudes varying with the target scattering characteristics Freeman and Saatchi [2004]. Conversely, we lack a clear picture of the magnitude and nature of Faraday-induced errors in the interferometric phase and hence estimates of deformation. The upcoming L-band InSAR satellite mission NISAR aims to estimate secular deformation with a high accuracy of better than 2 mm per year, which necessitates a sound understanding of even minor error terms.

Here, we focus on the errors in repeat-pass interferometric observations and deformation estimates. We attribute the Faraday-induced phase errors over distributed targets to contributions from the leakage of polarimetric phases into the interferometric phase and those due to interferometric phase diversity [Zwieback and Hajnsek, 2016], the polarimetric variability of the interferometric phase. We show that the relative importance and overall magnitude of the errors vary systematically with land cover and topography. The systematic nature of these errors further increases the need to understand and quantify the phase errors and their impact in geodetic studies.

To assess the magnitude and nature of the errors, we combine theoretical analyses with an empirical quantification for a range of land covers using L-band observations with simulated Faraday rotation. For the co-pol and the cross-pol channels, we quantify the errors in the observed interferometric phase ϕ and in the split-spectrum ionospherically corrected phase ϕ^c. Both are relevant to deformation analyses [Gomba et al., 2016], as the Faraday-induced errors in the displacement estimates will closely follow those in ϕ and ϕ^c on small and large spatial scales, respectively. We further determine the temporal characteristics of these systematic errors by simulating multi-annual time series for deformation analysis. Based on these theoretical and empirical results, we appraise the relevance of these hitherto neglected systematic errors for measuring deformation from space.

2 Theoretical considerations

2.1 Interferometric covariance matrix

The ionospheric Faraday effect alters the microwave signals a radar satellite receives and hence the apparent scattering properties of the Earth's surface. Mathematically, this influence can be expressed as an equivalence transformation applied to the interferometric covariance matrix $\mathbf{C}$:

$$_F\mathbf{C}(\chi_1, \chi_2) = \begin{bmatrix} \mathbf{R}_F(\chi_1) & \\ & \mathbf{R}_F(\chi_2) \end{bmatrix} \begin{bmatrix} \mathbf{\Sigma}_1 & \mathbf{\Omega} \\ \mathbf{\Omega}^\dagger & \mathbf{\Sigma}_2 \end{bmatrix} \begin{bmatrix} \mathbf{R}_F(\chi_1) & \\ & \mathbf{R}_F(\chi_2) \end{bmatrix}^T \tag{1}$$

where

$$\mathbf{R}_F(\chi) = \begin{bmatrix} \cos(2\chi) & 0 & 0 & -\sin(2\chi) \\ 0 & 1 & 0 & 0 \\ 0 & 0 & 1 & 0 \\ \sin(2\chi) & 0 & 0 & \cos(2\chi) \end{bmatrix}$$

is a unitary matrix [Wright et al., 2003, Freeman and Saatchi, 2004]. $\mathbf{\Sigma}_1$ and $\mathbf{\Sigma}_2$ are the polarimetric covariance matrices of acquisitions 1 and 2, respectively, whereas the off-diagonal block $\mathbf{\Omega}$ contains the interferometric information. Eq. 1 is given in the Pauli basis of the quad-pol scattering vector [Cloude and Pottier, 1996] in the backscattering alignment convention:

$$\mathbf{k} = \frac{1}{\sqrt{2}} \begin{bmatrix} S_{\text{HH}} + S_{\text{VV}} & S_{\text{HH}} - S_{\text{VV}} & S_{\text{HV}} + S_{\text{VH}} & i(S_{\text{HV}} - S_{\text{VH}}) \end{bmatrix}^T \tag{2}$$

The Faraday-affected interferometric phase $_F\phi$ for polarimetric measurement functionals $\mathbf{w}_1^\dagger$ and $\mathbf{w}_2^\dagger$ – linear functionals are denoted by row vectors that act through the standard inner product – is then given by

$$_F\phi = \arg\left(\mathbf{w}_1^\dagger \mathbf{R}_F(\chi_1) \mathbf{\Omega} \mathbf{R}_F^T(\chi_2) \mathbf{w}_2 \right). \tag{3}$$

To isolate purely interferometric signals from what are essentially polarimetric phase contributions [Cloude and Papathanassiou, 1998], one typically chooses $\mathbf{w}_1^\dagger = \mathbf{w}_2^\dagger \equiv \mathbf{w}^\dagger$ to obtain a phase $\phi_{\mathbf{w}\dagger}$. In presence of unequal Faraday rotation, however, the observed interferometric phase, $_F\phi_{\mathbf{w}\dagger}$, can be contaminated by polarimetric contributions. It can be thought of as the result of observing the original covariance matrix $\mathbf{C}$ with effective functionals $_F\mathbf{w}^\dagger = \mathbf{w}^\dagger \mathbf{R}_F(\chi_\cdot)$.

2.2 Phase errors

Two phenonema contribute to the Faraday-induced interferometric phase error,

$$_F\delta\phi_{\mathbf{w}\dagger} \equiv {}_F\phi_{\mathbf{w}\dagger} - \phi_{\mathbf{w}\dagger}. \tag{4}$$

The first one is the polarimetric leakage described above. It is only present for $\chi_1 \neq \chi_2$. The second one arises from phase diversity: the dependence of the Faraday-unaffected $\phi_{\mathbf{w}\dagger}$ on the polarimetric functional $\mathbf{w}^\dagger$. It induces errors even when $\chi_1 = \chi_2 \neq 0$. We have summarized the key theoretical properties of the error types in Tab. 1.

Polarimetric leakage is a confounding of the interferometric phase signal with polarimetric phase contributions. The spurious phase contributions are polarimetric in the sense that, for a perfectly coherent target, they originate from polarimetric phases. These polarimetric phases leak into the inteferometric phase when $\chi_1 \neq \chi_2$, as one essentially employs two distinct polarimetric channels $_F\mathbf{w}_1^\dagger \neq {}_F\mathbf{w}_2^\dagger$ to form the interferogram. Conversely, the phase error due to polarimetric leakage, $_F\delta\phi_{\mathbf{w}\dagger}^{\text{pol}}$, vanishes whenever $\chi_1 = \chi_2$ for any $\mathbf{\Omega}$ that does not exhibit phase diversity (i.e., that is phase invariant, see Sec. 7). To see this, we express the error in terms of the phase-free $\tilde{\mathbf{\Omega}}$

$$_F\delta\phi_{\mathbf{w}\dagger}^{\text{pol}} = \arg\left(\mathbf{w}^\dagger \mathbf{R}_F(\chi_1) \tilde{\mathbf{\Omega}} \mathbf{R}_F^T(\chi_2) \mathbf{w} \right). \tag{5}$$

2

Table 1: Summary of theoretical results. The total Faraday-induced phase error $_F\delta\phi_{\mathbf{w}^\dagger}$ from Eq. 4 is due to polarimetric leakage and phase diversity. The split-spectrum error Eq. 13 is the total error of the ionospherically corrected phase ϕ^c.

Error type	Property of Faraday-induced error
Polarimetric leakage $_F\delta\phi^{\mathrm{pol}}$	defined for phase-invariant $\mathbf{\Omega}$ vanishes for $\chi_1 = \chi_2$ co-pol: $_F\delta\phi^{\mathrm{pol}} \sim \chi_1^2 - \chi_2^2$, cross-pol: $\sim \chi_1 - \chi_2$ cross-pol: vanishes for reflection symmetry across $\mathcal{P}_V$ systematic accumulation over interferogram chains
Phase error $_F\delta\phi$	$\mathbf{\Omega}$ generally not phase invariant nonlinear combination of phase diversity and polarimetric leakage does not vanish when $\chi_1 = \chi_2$ leading order of χ dependence: 2 (co-pol) and 1 (cross-pol)
Split-spectrum errors $_F\delta\phi^c$	same order of magnitude as $_F\delta\phi$ for $\Delta f' \ll 1$

As $\tilde{\mathbf{\Omega}}$ is Hermitian positive (semi-)definite, $_F\delta\phi_{\mathbf{w}^\dagger} = 0$ for $\chi = \chi_1 = \chi_2$, or undefined whenever $\mathbf{R}_F^T(\chi)\mathbf{w}$ is in the null space of $\tilde{\mathbf{\Omega}}$. Even if the difference in χ is small for individual short-term interferograms, the polarimetric leakage errors tend to accumulate across interferogram chains (Sec. 8).

The influence of phase diversity can be seen most clearly when $\chi_1 = \chi_2$. Essentially, one forms an interferogram in the wrong interferometric channel $\mathbf{w}^\dagger \neq {}_F\mathbf{w}^\dagger$ for $\chi_1 = \chi_2 \neq 0$. Its phase will then be different from that of the correct interferometric channel unless $\mathbf{\Omega}$ obeys phase invariance.

Whenever $\mathbf{\Omega}$ displays phase diversity and $\chi_1 \neq \chi_2$, the total phase error cannot be neatly decomposed into contributions due to phase diversity and those due to polarimetric leakage. They are both present at the same time and interact nonlinearly on $_F\delta\phi_{\mathbf{w}^\dagger}$.

2.2.1 Co-pol phase errors

Expressing $\mathbf{\Omega}$ in the Pauli basis and assuming reciprocity in the absence of Faraday rotation [Cloude and Pottier, 1996], one obtains from Eq. 4

$$_F\phi_{\mathrm{HH/VV}} = \arg\left[\Omega_{22} + \Omega_{11}\cos(2\chi_1)\cos(2\chi_2) \pm \Omega_{12}\cos(2\chi_1) \pm \Omega_{21}\cos(2\chi_2)\right]. \tag{6}$$

The error with respect to the Faraday-free phase, $\phi_{\mathrm{HH/VV}}$, is of second order in the Faraday rotation angles

$$\begin{aligned} _F\delta\phi_{\mathrm{HH/VV}} &= {}_F\phi_{\mathrm{HH/VV}} - \phi_{\mathrm{HH/VV}} \\ &= \mp 2\frac{\mathrm{Im}\left(t_c\Omega_{12}\right)\chi_1^2 + \mathrm{Im}\left(t_c\Omega_{21}\right)\chi_2^2}{\mathrm{Re}\left(t_c\left(\Omega_{11} + \Omega_{22} \pm \Omega_{12} \pm \Omega_{21}\right)\right)} + o\left(\chi^3\right), \end{aligned} \tag{7}$$

using $t_c = e^{-i\phi_{\mathrm{HV/VV}}}$ and assuming phase wrapping is not an issue. The co-pol phase error for general $\mathbf{\Omega}$ does not vanish when $\chi_1 = \chi_2$, which is illustrated in Fig. 1a for an agricultural field. This is because it contains phase diversity and polarimetric leakage components.

The polarimetric leakage error for phase-invariant $\mathbf{\Omega}$ is

$$_F\delta\phi^{\mathrm{pol}}_{\mathrm{HH/VV}} = \mp 2\frac{\mathrm{Im}\left(\tilde{\Omega}_{12}\right)\left(\chi_1^2 - \chi_2^2\right)}{\tilde{\Omega}_{11} + \tilde{\Omega}_{22} \pm 2\mathrm{Re}\left(\tilde{\Omega}_{12}\right)} + o\left(\chi^3\right). \tag{8}$$

The leading-order term $\chi_1^2 - \chi_2^2$ induces an asymmetry in the Faraday-induced error (Fig. 1a). For fixed $\chi_1 > 0$, $_F\delta\phi^{\mathrm{pol}}_{\mathrm{HH/VV}}$ increases more rapidly in magnitude for $\chi_2 > \chi_1$ than it does for $\chi_2 < \chi_1$. The error vanishes when $\chi_1 = \chi_2$.

The polarimetric origin of this error is most evident when $\tilde{\mathbf{\Omega}} = \mathbf{\Sigma}_1 = \mathbf{\Sigma}_2 \equiv \mathbf{\Sigma}$, i.e. in absence of any interferometric changes between acquisitions one and two (other than Faraday rotation). The error is controlled by $\mathrm{Im}(\Sigma_{12})$. This term, along with the associated [Cloude et al., 2018] phase $\arg(\Sigma_{12})$, can be difficult to predict when both surface and volume scattering are appreciable. Simple models, such as the small-perturbation model for surface scattering and volume models with azimuthal symmetry [Cloude and Pottier, 1996], predict a small (compared to Σ_{11}) or even vanishing magnitude, and are thus prone to underestimating its size. Azimuth slopes θ reduce the $\mathrm{Im}(\Sigma_{12})$ term by $\cos 2\theta$ for an otherwise reflection-symmetric target [Lee and Ainsworth, 2011], so that flat terrain is expected to have comparatively large co-pol polarimetric leakage errors.
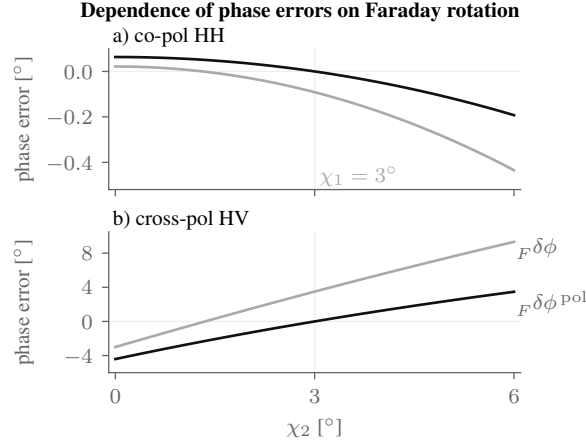
Dependence of phase errors on Faraday rotation

a) co-pol HH

b) cross-pol HV

Figure 1: Faraday-induced phase errors $_F\delta\phi$ for general $\mathbf{\Omega}$ and the polarimetric leakage errors $_F\delta\phi^{\text{pol}}$ for phase-invariant $\mathbf{\Omega}$ are shown for an agricultural field in a) HH and b) HV polarization. χ_1 was set to $3°$. The $\mathbf{\Omega}$ observation was taken from stack `31606` (Tab. 2); the phase-invariant component was computed from the Hermitian/skew-Hermitian decomposition (Sec. 3.3)

2.2.2 Cross-pol phase errors

For a reciprocal target, the cross-pol phase error from Eq. 4 can be expressed as

$$_F\phi_{\text{HV/VH}} = \arg\left[\Omega_{33} + \Omega_{11}\sin\left(2\chi_1\right)\sin\left(2\chi_2\right) \mp \Omega_{13}\sin\left(2\chi_1\right) \mp \Omega_{31}\sin\left(2\chi_2\right)\right]. \tag{9}$$

Faraday rotation thus induces first-order errors with respect to $\phi_{\text{HV}} = \phi_{\text{VH}}$, viz.

$$_F\delta\phi_{\text{HV/VH}} = \mp 2\frac{\text{Im}\left(t_x\Omega_{13}\right)\chi_1 + \text{Im}\left(t_x\Omega_{31}\right)\chi_2}{\text{Re}\left(t_x\left(\Omega_{33}\right)\right)} + o\left(\chi\right), \tag{10}$$

using $t_x = e^{-i\phi_{\text{HV}}}$. For fixed χ_1, the error can be approximated by a linear function in χ_2 near χ_1 (Fig. 1b).

The cross-pol errors are expected to be small for flat terrain, or more precisely for targets with reflection symmetry across the plane $\mathcal{P}_V$ formed by the line of sight and the vertical polarization direction [Lee and Ainsworth, 2011]. This is because i) polarimetric leakage is zero due to $\Omega_{13} = \Omega_{31} = 0$ [Cloude and Pottier, 1996], and ii) the phase-diversity error arising from $\arg(\Omega_{33}) \neq \arg(\Omega_{11})$ is only of second order in χ.

Conversely, the errors can be substantial when the terrain is tilted in azimuth. To estimate the polarimetric leakage, consider first a horizontal target that is reflection symmetric across $\mathcal{P}$ with phase-invariant $\tilde{\mathbf{\Omega}}^r$. If that target is tilted by θ in azimuth, the polarimetric leakage error increases with θ as

$$_F\delta\phi_{\text{HV/VH}}^{\text{pol}} = \pm 2\frac{\sin(2\theta)\text{Im}\left(\tilde{\Omega}_{12}^r\right)}{\tilde{\Omega}_{22}^r\sin(2\theta)^2 + \tilde{\Omega}_{33}^r\cos(2\theta)^2}\left(\chi_1 - \chi_2\right) + o(\chi). \tag{11}$$

The rate at which the error increases with θ is determined by the ratio of the imaginary part of $\tilde{\Omega}_{12}^r$ and the cross-pol magnitude $\tilde{\Omega}_{33}^r$. For sparsely vegetated areas, the low magnitude and coherence of the cross-pol return will tend to increase this ratio and hence accentuate phase errors in rolling terrain.

2.3 Split-spectrum errors

2.3.1 Split-spectrum correction

Split-spectrum analyses serve to estimate and remove the ionospheric phase screen [Brcic et al., 2010, Gomba et al., 2016]. Their rationale is to exploit the dispersive nature of the ionospheric phase screen by quantifying interferometric phase differences across spectral sub-bands [Appleton and Builder, 1933].

Faraday rotation may bias split-spectrum analyses when the Faraday-induced $_F\delta\phi$ in the sub-bands propagate to the ionospherically corrected phase. The bias in turn depends on how $_F\delta\phi$ changes with frequency. Frequency-dependent $_F\delta\phi$ arises because i) Faraday rotation angles [Wright et al., 2003] and ii) the $\mathbf{\Omega}$ matrix (other than multiplication by a scalar) vary with frequency.

A potential additional iii) source of frequency-dependent errors are differences in polarization. In the quasi-quadpol mode under consideration for NISAR, the HH–HV main band would be complemented by a VV–VH sideband [Kellogg et al., 2020].

Then, differences in polarization that arise directly from phase diversity (e.g. an HH–VV phase difference associated with birefringence in agricultural canopies [Zwieback and Hajnsek, 2016]) or from the polarization-dependent impact of Faraday rotation (e.g. HV vs. VH) could bias the ionospheric correction.

Our theoretical analyses focus on the errors in the ionosphere-corrected phase ϕ^c at frequency $f = f_0$ obtained by split-spectrum analysis [Gomba et al., 2016]. The spectrum is split into a lower band with $f = f'_- f^0$ and an upper band with $f = f'^+ f_0 \equiv (f'^- + \Delta f')f^0$, whose interferometric phase observations are denoted as ϕ^- and ϕ^+, respectively. The corrected phase ϕ^c is given by [Brcic et al., 2010]

$$\phi^c = \frac{\phi^+ f'^+ - \phi^- f'^-}{\Delta f' \ (f'^+ + f'^-)} \ .\tag{12}$$

There is a certain ambiguity in the corrected phase ϕ^c and in ionospheric corrections more generally. For non-zero Faraday rotation, the ionospheric delay and phase screen are not scalars [Hartmann and Leitinger, 1984]. We adopt Kim et al. [2015]'s convention that the 'correct' way to remove the ionospheric phase screen corresponds to the removal of the ionospheric phase delay that a pure idealized dihedral (Pauli 2), pure cross-pol (Pauli 3), or a pure helical scatter would experience. This delay is also what would be measured for a pure single bounce (Pauli 1) observed with a Pauli 1 $\mathbf{w}$. As a metric of the ambiguity, we define $\Gamma = 2|\chi_2 - \chi_1|$, the magnitude of the deviation in the interferometric phase delay between a pure Left-Right (LR) or an RL scatterer, neither of which is reciprocal.

The corrected phase ϕ^c is more of theoretical than of practical value. In practice, it can only be estimated at the reduced resolution of ϕ^- and ϕ^-. To retain the full resolution, actual implementations instead subtract a smoothed split-spectrum ionospheric estimate from the full-resolution phase. The two corrections are equivalent when the scattering characteristics are uniform across the ionospheric smoothing filter. With our focus on ϕ^c, we thus implicitly concentrate on homogeneous environments. Conversely, at length scales smaller than the filter size, the Faraday-induced error will be dominated by that of the raw phase, $_F\delta\phi$.

2.3.2 Error analysis

The split-spectrum ionospheric corrected phase is impacted by frequency-varying and frequency-invariant phase errors to a different extent [Gomba et al., 2016], as for general errors $\delta\phi$ it follows from Eq. 12 that

$$\delta\phi^c = \frac{\left(\delta\phi^+ - \delta\phi^-\right) f'^- + \delta\phi^+ \Delta f'}{\Delta f' \left(2f'^- + \Delta f'\right)} \ .\tag{13}$$

Roughly speaking, frequency-invariant errors are halved, whereas differences between the bands $\Delta\delta = \delta\phi_+ - \delta\phi_-$ get amplified substantially, by a factor of $\approx (2\Delta f')^{-1}$.

The contributions from frequency-varying and frequency-invariant Faraday errors to $\delta\phi^c$ are of the same order of magnitude. This is because $\Delta\delta$ is small, as it generally scales as $\Delta f'$. We consider identical sub-band polarizations and assume that i) the frequency-dependence of Faraday errors is the only cause for diverging Faraday-induced errors in the sub-bands. As $\chi \sim f'^{-2}$ [Jokipii and Lerche, 1969], $\Delta\delta \sim 2\Delta f'$ in the cross-pol channel (first-order scaling of the Faraday errors), while it is proportional to $4\Delta f'$ for the co-pol channel (second-order errors).

The Faraday error in the corrected phase ϕ^c and the raw phase ϕ are of the same order of magnitude, provided that the same polarization is used for both subbands. This is because the frequency-varying and frequency-invariant contributions are of the same order of magnitude, the latter corresponding to the error of the raw phase. If the two contributions are of opposite sign, partial cancellation can occur.

A radically different picture emerges for quasi-quadpol systems. The inter-band error $\Delta\delta$ is then also due to iii) polarization differences, and its potentially large magnitude gets further amplified by a large factor of approximately $(2\Delta f')^{-1}$.

3 Observational analyses

3.1 Faraday-free radar observations

We studied five fully polarimetric SLC stacks, summarized in Tab. 2, acquired by NASA's L-band UAVSAR system [Fore et al., 2015]. We formed the interferometric covariance matrix by boxcar multilooking using $L = 100$ looks, obtaining a resolution of ~ 10 m. We enforced scattering reciprocity by setting the Pauli 4 return to zero. These airborne data are not affected by ionospheric distortions.

3.2 Quantifying phase errors by adding Faraday rotation

To estimate the Faraday-induced co-pol and cross-pol phase errors $_F\delta\phi$, we simulated Faraday-affected interferometric pairs with a temporal baseline of 1–3 weeks using (1). The phase errors $_F\delta\phi$ were estimated by subtracting the Faraday-unaffected from the Faraday-affected phase.

Table 2: The location, dominant land cover, UAVSAR stack number, and the number $N.$ of studied regions of interest with crops, sparse vegetation or forest cover, respectively.

Location			Stack	Land cover	N_c	N_s	N_f
California, USA	31.1N	122.2W	05508	semiarid scrub, wetland	0	3	0
Manitoba, Canada	49.6N	98.0W	31606	fields: cereals, oilseeds	5	0	1
Quebec, Canada	46.8N	71.1W	18801	forest, clearcuts, fields	1	2	2
Maine, USA	45.1N	68.6W	16701	mixed forest	0	0	4
Estuaire, Gabon	0.5N	9.5E	27080	tropical rain forest	0	0	1

The Faraday rotation angles χ_1 and χ_2 were chosen to cover the range of potential values at L-band [Freeman and Saatchi, 2004]. For most analyses, we focused on four values, namely $0°$ (none), $3°$ (weak), $10°$ (strong), and $30°$ (maximum).

3.3 Magnitude and nature of Faraday-induced phase errors

To assess how the Faraday-induced errors vary with land cover, we summarized the mean $_F\delta\phi$ values for each interferogram across multiple regions of interest for three land cover classes (Tab. 2): agricultural (pronounced phase diversity), sparsely vegetated (scrub, wetlands, clearcuts), and forest.

To quantify the $_F\delta\phi$ contribution from polarimetric leakage relative to that induced by phase diversity, we estimated $_F\delta\phi^{\mathrm{pol}}$ for a phase-invariant approximation $\tilde{\boldsymbol{\Omega}}$ derived from the observed $\boldsymbol{\Omega}$ as follows. We first computed

$$\boldsymbol{\Omega}' = \frac{\mathrm{tr}\left(\boldsymbol{\Omega}\right)^*}{|\mathrm{tr}\left(\boldsymbol{\Omega}\right)|}\boldsymbol{\Omega}, \tag{14}$$

which would be a positive (semi-)definite Hermitian matrix if $\boldsymbol{\Omega}$ were phase invariant to begin with. From the Hermitian/skew-Hermitian decomposition of $\boldsymbol{\Omega}'$, we extracted Hermitian component, setting any negative eigenvalues to zero.

We assessed the association of the cross-pol errors with deviations from reflection symmetry. We estimated the orientation angle θ for tilted reflection-symmetric targets [Lee and Ainsworth, 2011] and the Pauli 1–Pauli 3 polarimetric coherence $\rho_{13} = |\Sigma_{13}|\left(\Sigma_{11}\Sigma_{33}\right)^{-\frac{1}{2}}$, which is zero for reflection symmetry across $\mathcal{P}_V$.

3.4 Simulated temporal evolution of Faraday-induced errors

The temporal evolution of the Faraday-induced phase error was simulated using Faraday rotation angles χ derived from the International GNSS Service (IGS) TEC products. We extracted the final combined IGS TEC [Hernández-Pajares et al., 2009] estimate evaluated at the site of the Californian UAVSAR stack at 5 pm local time every 11 days, roughly corresponding to the late afternoon acquisitions of a sun-synchronous satellite. From these TEC estimates, we computed χ using the expression by Wright et al. [2003] for a polar L-band satellite with an incidence angle of $30°$.

We estimated the Faraday-induced errors with respect to the first acquisition due to polarimetric leakage alone, $_F\delta\phi^{\mathrm{pol}}$, using a fixed phase-invariant $\boldsymbol{\Omega}$ derived from the UAVSAR observations. We focused on the polarimetric leakage error because it is often the dominant contribution, and because we lack long-term observations to characterize the phase diversity adequately. Furthermore, by using a single phase-invariant covariance matrix, the impact of the arbitrary choice of adding up 11-day interferograms to obtain a long time series is small for dominant surface scattering. This is because polarimetric leakage does not induce closure errors [Zwieback et al., 2016] for rank-one $\boldsymbol{\Omega}$ (see Sec. 8).

3.5 Split-spectrum errors

We estimated the impact of Faraday rotation on the split-spectrum ionospheric correction for an L-band system such as NISAR [Kellogg et al., 2020]. The system parameters were given by $f^0 = 1.243$ GHz, $f'^- = 1.0$, $f'^+ = 1.02$. We assumed that $\boldsymbol{\Omega}(f') = \exp \mathrm{i}\phi\left(f'\right))\boldsymbol{\Omega}(f^0)$, thus neglecting changes in intensity, polarimetric phases, and coherence magnitudes as well as in polarimetric interferometric phase differences with frequency. We further assumed the interferometric phase differences between any two $\mathbf{w}^\dagger$ were less than 2π in magnitude. Under these assumptions, we assessed the split-spectrum phase errors for same-polarization split-spectrum analyses (HH, HV) but also for the quasi-quadpol mode combinations proposed for NISAR (HH-VV, HV-VH).

The error due to Faraday rotation, $_F\delta\phi^c$, was computed using (13) from the $_F\delta\phi$ phase errors in the two bands. For the quasi-quadpol configurations, we also computed the total error, which is due to Faraday rotation and the polarimetric interferometric phase difference between the polarization of the $-$ and the $+$ band, $\Delta\phi$. This total error of the corrected phase, $_T\delta\phi^c$, was obtained by setting the error in ϕ^+ to $_T\delta\phi^+ = {_F\delta\phi^+} - \Delta\phi$.
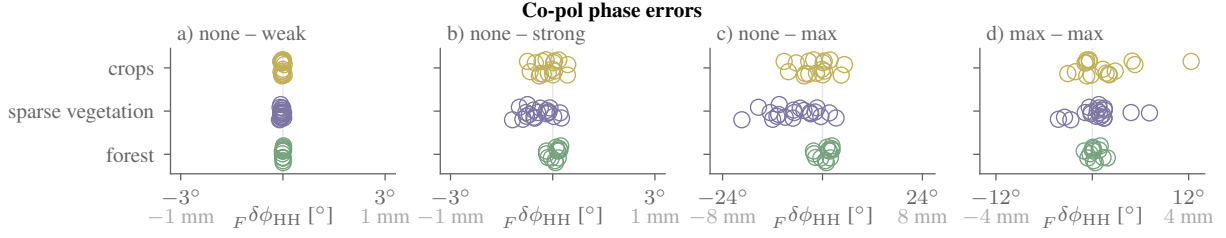
Co-pol phase errors

Figure 2: Faraday-induced phase errors at HH across multiple regions of interest for four different Faraday rotation combinations $\chi_1 - \chi_2$ (none, weak, strong, and max are $0°$, $3°$, $10°$, and $30°$, respectively). The corresponding deformation error is shown in grey.
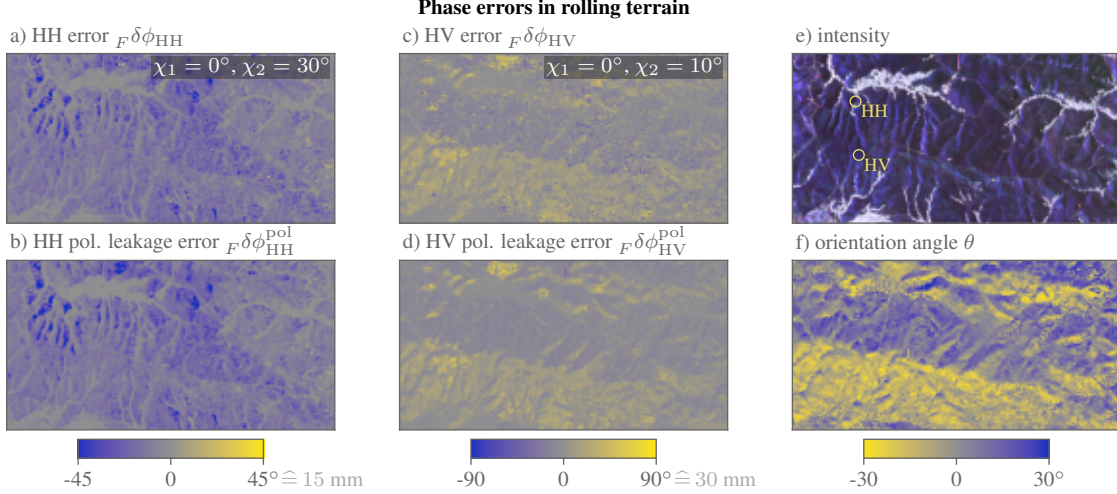

Phase errors in rolling terrain

Figure 3: Faraday-induced phase errors in rolling, predominantly sparsely vegetated terrain near Vallejo, California. The look direction is from the left. a) Error in HH for maximum Faraday rotation $\chi_2 = 30°$; b) HH error predicted just due to polarimetric leakage; c–d) same as a–b) but in HV for strong Faraday rotation $\chi_2 = 10°$; e) Pauli RGB composite showing sparsely vegetated hillslopes and ridges in dark, blueish tones and densely vegetated valleys in white, while the yellow circles indicate the locations shown in Fig. 6; f) polarimetric orientation angle θ.

4   Results

4.1   Co-pol phase errors

The co-pol phase errors induced by Faraday rotation are expected to be small or moderate unless ionospheric Faraday rotation is exceptionally large (Fig. 2a–d). The predicted magnitude of $_F\delta\phi$ at HH remains below $3°$, or 1 mm, for an increase in Faraday rotation from $\chi_1 = 0°$ to $\chi_2 = 3°$ and $10°$. It is only when the difference in Faraday rotation is large, $\chi_2 = 30°$ that $|_F\delta\phi|$ in excess of $6°$ (2 mm) are predicted. For maximum $\chi = 30°$, the errors are appreciable (Fig. 2d) even when there is no difference in Faraday rotation, $\chi_1 = \chi_2$.

The errors are most pronounced for agricultural fields and for sparsely vegetated slopes. In sparsely vegetated terrain, large phase errors are predominantly associated with polarimetric leakage. The $_F\delta\phi^{\mathrm{pol}}$ due to polarimetric leakage alone can largely predict the spatial patterns of $_F\delta\phi$ in hilly terrain in the San Francisco Bay area (Fig. 3a–b). The dominance of polarimetric leakage also applies to bare surfaces observed at grazing incidence angles. Large negative values $_F\delta\phi \sim -45°$, corresponding to deformation errors of 15 mm, prevail for maximum Faraday rotation $\chi_2 = 30°$ (Fig. 3a–b). The large magnitudes are associated with $\arg(\Sigma_{12}) \sim -140°$ and a high polarimetric correlation of ~ 0.8. Over agricultural fields during the growing season, the errors vary from field to field in a way that can largely but not entirely be explained by polarimetric leakage (Fig. 4a–b). The pronounced phase diversity shown in Fig. 4f) also contributes to the errors. The contribution of phase diversity to the Faraday-induced errors over croplands is evident for $\chi_1 = \chi_2$ (Fig. 2d).

7

Phase errors in flat agricultural terrain

a) HH error $_F\delta\phi_{HH}$

c) HV error $_F\delta\phi_{HV}$

e) ρ_{13} polarimetric coherence

b) HH pol. leakage error $_F\delta\phi_{HH}^{pol}$

d) HV pol. leakage error $_F\delta\phi_{HV}^{pol}$
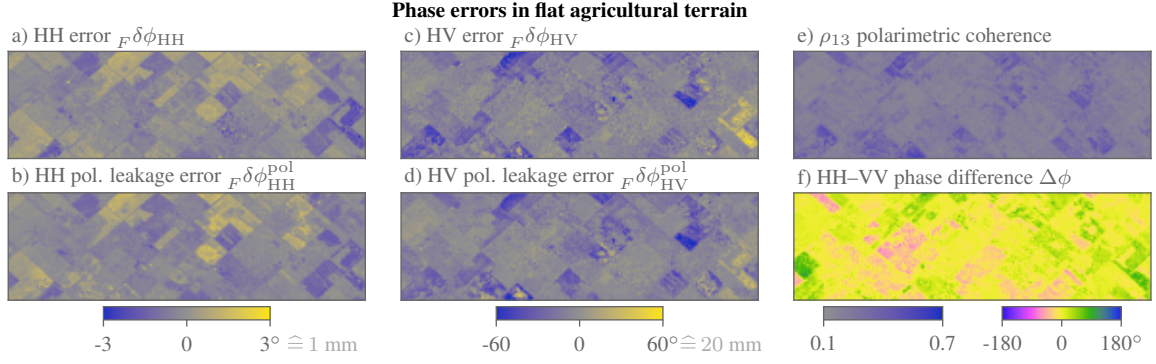
f) HH–VV phase difference $\Delta\phi$

Figure 4: Faraday-induced phase errors in a flat agricultural landscape near Carman, Winnipeg. The look direction is from below. a, c) Error in HH and HV respectively for strong Faraday rotation $\chi_2 = 10°$ while $\chi_1 = 0°$; b, d) errors predicted just due to polarimetric leakage; e) elevated ρ_{13} [-] for certain fields despite the low relief; f) HH–VV interferometric phase difference can be substantial for rapidly changing crops.

Cross-pol phase errors

a) none – weak

b) none – strong
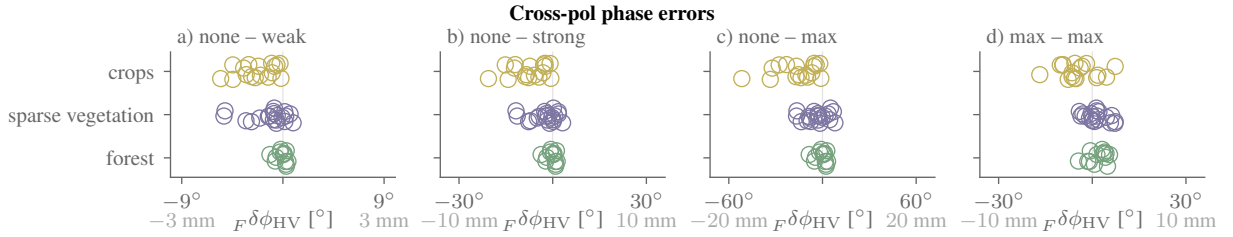
c) none – max

d) max – max

Figure 5: Faraday-induced phase errors at HV across multiple regions of interest for the same four different Faraday rotation combinations $\chi_1 - \chi_2$ as in Fig. 2

4.2 Cross-pol phase errors

Faraday rotation can readily induce substantial cross-pol phase errors in individual interferograms. For $\chi_1 = 0°$ and small $\chi_2 = 3°$, the predicted magnitudes are shown in Fig. 5 to reach values up to 6°, or 2 mm. For strong and maximum Faraday rotation in the second acquisition, the deformation errors can exceed 10 mm. Errors of comparable magnitude are also obtained when the Faraday rotation is very large but constant.

Particularly large errors are expected in moderate to high-relief terrain. Azimuth slopes increase the error magnitude, and the error sign also reflects the azimuth slope, as the polarimetric leakage scales with $\sin(\theta)$ for reflection-symmetric targets according to (11). For the sparsely vegetated rolling terrain in in Fig. 3, the error due to polarimetric leakage $_F\delta\phi^{pol}$ dominates the error and its close association with topography.

Even in flat terrain such as that in Fig. 4, polarimetric leakage and phase diversity can induce substantial $_F\delta\phi_{HV}$. Despite the low relief, the ρ_{13} polarimetric coherence in Fig. 4e indicates prominent deviations from reflection symmetry across $\mathcal{P}_V$ in croplands [Zwieback and Hajnsek, 2014], which enable substantial errors due to polarimetric leakage.

4.3 Simulated temporal evolution of Faraday-induced errors

The Faraday rotation angle χ derived from the IGS TEC product and the simulated errors exhibit complex temporal patterns around the 2002 solar maximum. Figure 6 shows the simulated errors due to polarimetric leakage, $_F\delta\phi^{pol}$, for the two locations annotated in Fig. 3e. Both are sparsely vegetated and on slopes: at HH, the slope faces away from the instrument, while at HV it is mainly in the azimuth direction. As the polarimetric leakage errors are large for these two locations, the simulations constitute a pessimistic scenario for rolling, sparsely vegetated terrain in California.

The magnitude of the simulated errors is not negligible compared to the desired millimetric geodetic accuracy on semi- to multi-annual time scales. The maximum magnitude differs substantially between the co-pol (HH) and cross-pol (HV) observations. The semi-annual and multi-annual co-pol phase errors are $\sim 5°$, corresponding to 2 mm. The cross-pol errors are 5 times as large.

The temporal patterns are different for the two polarizations. This is largely due to the differences in the dependence of the Faraday-induced errors on χ. At HH, the second-order impact (Tab. 1) of χ i) emphasizes the peak TEC ($\chi = 16°$) in
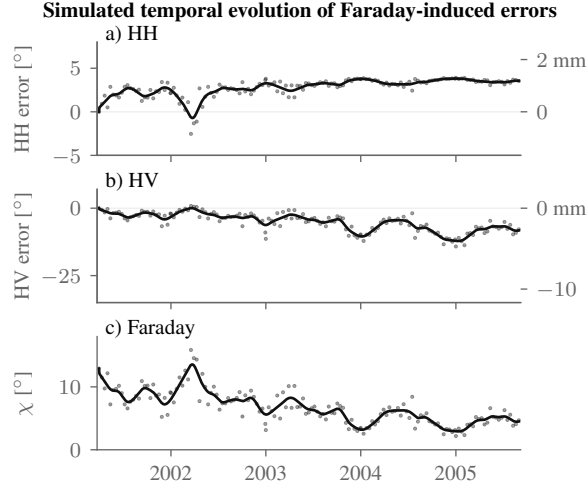
Figure 6: Simulated Faraday-induced phase errors due to polarimetric leakage in California around the 2002 solar maximum for the two locations shown in Fig. 3e. a) Simulated HH phase $_F\delta\phi_{HH}^{pol}$ (left) and displacement error (right); b) same for HV; c) Faraday angle χ estimated from the IGS ionospheric TEC product. The markers show the respective values at an interval of 11 days; the line is a smoothed monthly estimate.
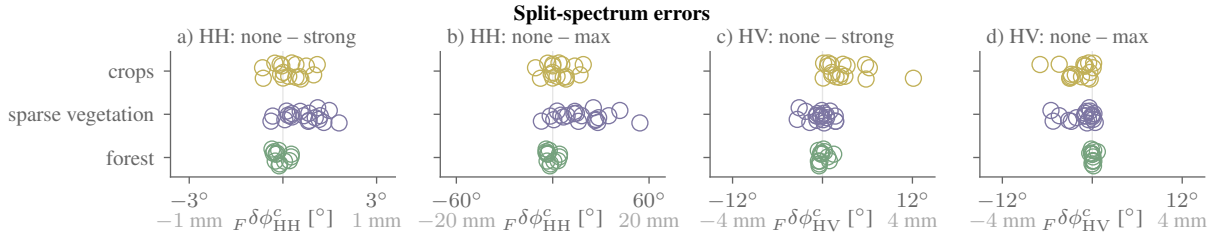

Figure 7: Faraday-induced errors in the split-spectrum ionospherically corrected phase at a–b) HH and c–d) HV across multiple regions of interest. The Faraday rotation combinations $\chi_1 - \chi_2$ overlap with those in Fig. 2

2002 and ii) dampens the annual variations at low TEC after 2004. Intuitively, the second-order scaling in Eq. 8 is equivalent to the product of the mean χ and their difference $\Delta\chi$. For a large initial $\chi_1 = 13°$, the second-order error thus i) emphasizes $\Delta\chi$ when both χ are large, and ii) dampens the influence of $\Delta\chi$ when the mean is small. Conversely, the leading first-order term at HV is i) less sensitive to the small increase in χ from 2001 to 2002, but it ii) amplifies the large difference to the TEC minima after 2004, aided by deviations from purely first-order scaling. To summarize, the Faraday-induced errors can exhibit complex patterns across time scales.

4.4 Split-spectrum errors

The errors in the ionospherically corrected phase associated with uncompensated Faraday rotation are generally of comparable magnitude to those in the uncorrected phase when the same polarization is used for the upper and lower band (Fig. 7).

For the co-pol channel HH, the error in the corrected phase, $_F\delta\phi^c$, is on the order of $2°$ for strong Faraday rotation ($\chi_1 = 0°$ and $\chi_2 = 10°$). It is thus substantially smaller than the inherent ionospheric delay phase ambiguity of $\Gamma = 20°$. For maximum Faraday rotation $\chi_2 = 30°$, the errors can exceed those of the uncorrected phase, reaching values of up to $60°$, or 20 mm.

For the cross-pol channel HV, the predicted error $_F\delta\phi^c$ can exceed $10°$ for certain croplands at $\chi_2 = 10°$. For maximum $\chi_2 = 30°$, the areas studied are subject to a compensation effect in that the $_F\delta\phi_c$ decrease in magnitude (and sometimes change sign) for increasing χ_2.

Faraday rotation severely compromises the quasi-quadpol split-spectrum ionospheric correction (Fig. 8). For the co-pol HH–VV band combination, the errors due to the Faraday rotation alone $_F\delta\phi^c$, shown in Fig. 8a, can exceed $30°$ for strong $\chi_2 = 10°$. However, much larger errors can be induced by the HH–VV phase difference itself, also in the absence of Faraday rotation. Phase differences $\phi_{HH} - \phi_{VV} \gtrsim 20°$, e.g. in croplands due to birefringence, get magnified to errors $_T\delta\phi^c \gtrsim 360°$, or 12 cm, in Fig. 8b. For the cross-pol HV–VH combination, the situation is different because the phase differences ϕ_{HV} and
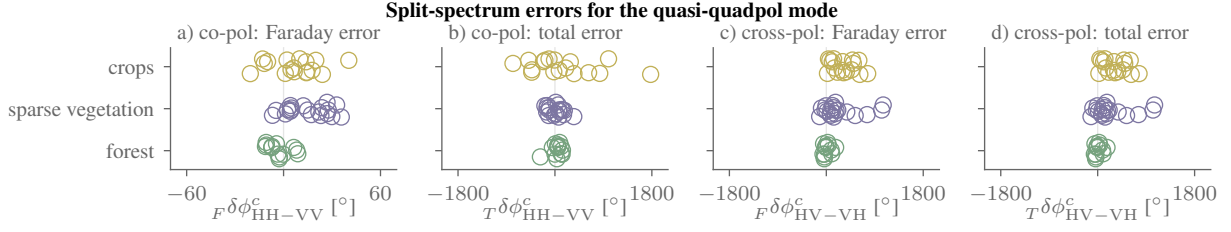
Figure 8: Faraday-induced errors in the split-spectrum ionospherically corrected phase in the quasi-quadpol mode for $\chi_1 = 0°$ (none) $- \chi_2 = 10°$ (strong). a and c) show the errors that are due to Faraday rotation alone for the HH–VV and the HV–VH band combinations, respectively. b and d) show the total error for the same combinations. Panels c) and d) are identical due to the enforced reciprocity of the Faraday-unaffected observations.

ϕ_{VH} are identical for reciprocal targets without Faraday rotation. The errors, which are exclusively due to Faraday rotation, nevertheless commonly exceed $360°$, or 12 cm, in Fig. 8c–d.

5 Discussion

5.1 Magnitude and nature of Faraday-induced phase errors

In the co-polar channels, Faraday-induced interferometric phase errors are often, but not always, small. For both the observed phase (Fig. 2a–c) and the split-spectrum ionospherically corrected phase (Fig. 7a), they are predicted to generally remain $\lesssim 3°$, or 1 mm at L-band. However, our analyses reveal two important exceptions for which errors can exceed 2 mm. First, barely vegetated slopes facing away from the radar and other locations whose polarimetric scattering characteristics (large imaginary part of the Pauli 12 component; 8) promote elevated Faraday-induced phase errors due to polarimetric leakage. Second, exceptionally large TEC values, which may for instance occur during strong solar maxima. The associated Faraday rotation angles (Fig. 2c) induce substantial errors of ∼5 mm.

For the cross-pol channel, Faraday-induced interferometric phase errors are a major concern (Fig. 5). The magnitude of the $_F\delta\phi$ errors can exceed $30°$, or 10 mm, even for Faraday rotation that is not exceptionally strong. Sparsely vegetated high-relief terrain is prone to large errors, as the errors contain a topographic signature induced by polarimetric leakage (Fig. 3). While phase diversity also contributes to the Faraday-induced phase errors, most markedly in agricultural areas, polarimetric leakage generally constitutes the dominant error source.

5.2 Relevance for measuring deformation

The Faraday-induced phase errors in the co-pol channels compel attention in geodetic analyses of deformation, chiefly for three reasons.

First, their magnitudes of ∼2 mm on semi- to multi-annual time scales (co-pol; Fig. 6b) are comparable to the accuracy requirements for the NISAR mission, which are 2 mm/year for secular deformation rates [Kellogg et al., 2020]. On shorter time scales, the errors may reach ∼1 cm for very large peak TEC and χ during a solar maximum (Fig. 2d, 3a).

Second, the temporal patterns, with pronounced variability on subseasonal and (semi)-annual time scales as well as persistent longer-term trends (Fig. 6), mimic those of deformation processes such as landslides or aseismic creep. They can thus systematically distort geophysical model inversions and interpretations.

Third, the spatial patterns of the errors also predispose to inappropriate interpretations. Their strong association with relief and landcover mimics that of deformation processes such as solifluction. In contrast to other atmospheric errors, the $_F\delta\phi$ errors can exhibit sharp boundaries (Fig. 3–4) because the ionospheric patterns are modulated by surface characteristics.

In summary, the error magnitudes in the co-pol channels are large enough to warrant consideration, compounded by their pernicious spatiotemporal characteristics.

5.3 Mitigating Faraday-induced errors in geodetic analyses

It would be desirable to correct the errors, but there is insufficient information to do so rigorously without quad-pol data. Even if the Faraday rotation were known accurately, error correction requires estimates of interferometric scattering terms that are unobserved and difficult to predict.

A less ambitious goal than error correction is to flag large Faraday-induced errors. Such flagging needs to account for both factors conducive to large errors: elevated TEC and adverse scattering characteristics. Discarding entire scenes with elevated

TEC irrespective of the scattering characteristics is akin to throwing out the baby with the bath water. The example of the 2002 solar maximum in Figure 6 illustrates that, due to persistent elevated TEC, not all compromised scenes can meaningfully be discarded.

Error correction and flagging is amenable to statistical approaches trained with quad-pol observations. The predictive skill of statistical correction models will likely benefit from external ionospheric, land cover, and topographic information (cf. Fig. 3). The interferometric phase differences between the co-pol and the cross-pol channels will be useful predictors for quantifying or flagging Faraday-induced phase errors.

6 Conclusions

Our theoretical and observational analyses show that phase errors induced by uncompensated Faraday rotation constitute an important and hitherto neglected error in interferometric deformation measurements. The typical magnitude is up to 2 mm in the co-pol channels at L-band, but it may exceed 5 mm for intense solar maxima [Wright et al., 2003] and surfaces with adverse scattering characteristics. The cross-pol channel is more prone to severe errors, which can exceed several centimeters.

These errors are systematic, as they can add up and persist over time. Their temporal characteristics, such as pronounced seasonal and quasi-decadal variability, are similar to those of common deformation processes. They are further strongly associated with the topography and land cover because they result from the modulation of ionospheric signals by surface scattering characteristics. They can largely be attributed to a leakage of polarimetric phases into the interferometric phase. Even when these errors remain subtle ($\sim 6°$ or 2 mm at L band), their systematic nature makes the spurious Faraday-induced patterns prone to being misinterpreted as deformation.

These errors cannot rigorously be corrected for in non-quad-pol systems because they depend on unobserved quantities. Statistical detection and mitigation approaches thus appear to be a promising avenue for error mitigation. Because these systematic errors cannot be removed rigorously, they deserve to be accounted for in error budgets and in quantitative analyses.

7 Appendix: Phase invariance / diversity

We define $\mathbf{C}$, or more narrowly an off-diagonal interferometric submatrix $\boldsymbol{\Omega}$, to obey phase invariance when for any two non-zero polarimetric functionals $\mathbf{w}_A^\dagger$ and $\mathbf{w}_B^\dagger$

$$\arg\left(\mathbf{w}_A^\dagger \boldsymbol{\Omega} \mathbf{w}_A\right) = \arg\left(\mathbf{w}_B^\dagger \boldsymbol{\Omega} \mathbf{w}_B\right) , \tag{15}$$

provided that $\mathbf{w}^\dagger \boldsymbol{\Omega} \mathbf{w} \neq 0$ for $\mathbf{w}_A^\dagger$ and $\mathbf{w}_B^\dagger$. We treat functionals for which $\mathbf{w}^\dagger \boldsymbol{\Omega} \mathbf{w} = 0$ as separate cases, i.e. they are assumed not to break phase invariance in and of themselves. Conversely, we speak of phase diversity whenever phase invariance does not hold.

Phase invariance
$\boldsymbol{\Omega}$ is phase invariant if and only if $\boldsymbol{\Omega}$ can be written as $e^{i\tilde{\phi}}\tilde{\boldsymbol{\Omega}}$ where $\tilde{\boldsymbol{\Omega}} = \tilde{\boldsymbol{\Omega}}^\dagger$ is positive semi-definite.

Proof for if
Provided $\mathbf{w}^\dagger \boldsymbol{\Omega} \mathbf{w} \neq 0$

$$\phi_{\mathbf{w}^\dagger} = \arg\left(e^{i\tilde{\phi}} \underbrace{\mathbf{w}^\dagger \tilde{\boldsymbol{\Omega}} \mathbf{w}}_{>0}\right) = \tilde{\phi} ,$$

which is independent of $\mathbf{w}^\dagger$.

Proof for only if:
Pick a $\mathbf{w}_\heartsuit^\dagger$ such that

$$\mathbf{w}_\heartsuit^\dagger \boldsymbol{\Omega} \mathbf{w}_\heartsuit = a_\heartsuit e^{i\phi_\heartsuit} ,$$

where $a_\heartsuit > 0$ is a positive real number. If one cannot pick such a $\mathbf{w}_\heartsuit^\dagger$, this can be shown to imply that $\boldsymbol{\Omega}$ is the zero matrix, in which case interferometric phases are not defined. Having found $\mathbf{w}_\heartsuit^\dagger$, we can write for general $\mathbf{w}^\dagger$

$$\phi_{\mathbf{w}^\dagger} = \arg\left(e^{i\phi_\heartsuit} \underbrace{\mathbf{w}^\dagger e^{-i\phi_\heartsuit} \boldsymbol{\Omega} \mathbf{w}}_{m(\mathbf{w}^\dagger)}\right) .$$

$$\tag{16}$$

Phase invariance implies that $m(\mathbf{w}^\dagger)$ must be real and ≥ 0. This in turn implies that $e^{-i\phi_\heartsuit} \boldsymbol{\Omega}$ is Hermitian (real) positive semidefinite (≥ 0). For any phase-invariant $\boldsymbol{\Omega}$, it thus follows that $\phi_\heartsuit = \tilde{\phi}$ and unique (modulo 2π). Furthermore, $\tilde{\boldsymbol{\Omega}} = e^{-i\tilde{\phi}} \boldsymbol{\Omega}$.

11

A complementary way of interpreting phase invariance is by relation to the coherence region and the numerical range [Neumann et al., 2006, Cui et al., 2015] of $\mathbf{\Omega}$, $W(\mathbf{\Omega})$. The set of all valid $\phi_{\mathbf{w}\dagger}$ is the image of $W(\mathbf{\Omega})$ under the argument function. If it is to collapse to a single value (phase invariance), $W(\mathbf{\Omega})$ must be contained in a ray. This in turn is equivalent to $\mathbf{\Omega}$ being a normal matrix whose eigenvalues all have the same argument [Murnaghan, 1932], viz. $\mathbf{\Omega} = e^{i\tilde{\phi}}\tilde{\mathbf{\Omega}}$ if we allow for zero eigenvalues.

8   Appendix II: Accumulation of polarimetric leakage errors

We show that the polarimetric leakage errors are temporally persistent across chains of interferograms: even if the Faraday rotation change and hence the error is small for short temporal baselines, long-term changes in Faraday rotation will induce systematic long-term errors.

We assume the phase-invariant $\mathbf{\Omega} = \tilde{\mathbf{\Omega}}$ is time invariant for nearest-neighbour interferograms. The total error when adding up nearest-neighbour interferograms

$$
\begin{aligned}
{}_F\delta\phi^{1\,2} + \cdots + {}_F\delta\phi^{(K-1)\,K} &= \sum_{k=1}^{K-1} \beta(\chi_k^n - \chi_{k+1}^n) + o(\chi^n) \\
&= \beta(\chi_1^n - \chi_K^n) + o(\chi^n)\,,
\end{aligned}
\tag{17}
$$

so that up to the leading order n (1 for cross-pol, 2 for co-pol), this would be equal to $\phi^{1\,K}$ if the latter had the same $\tilde{\Omega}$. To arbitrary order of accuracy, it is the single-interferogram error for an effective phase-diverse $\mathbf{\Omega}^e$

$$
\mathbf{\Omega}^e = \tilde{\mathbf{\Omega}}^{\frac{1}{2}}\mathbf{l}_2\mathbf{l}_2^{\dagger}\cdots\mathbf{l}_{K-1}\mathbf{l}_{K-1}^{\dagger}\tilde{\mathbf{\Omega}}^{\frac{1}{2}}\,,
\tag{18}
$$

where $\mathbf{l}_k \equiv \tilde{\mathbf{\Omega}}^{\frac{1}{2}}\mathbf{R}_F^T(\chi_k)\mathbf{w}$, and where $\tilde{\mathbf{\Omega}}^{\frac{1}{2}}$ is the Hermitian square root. Because variable χ_k maps variable polarimetric components in $\tilde{\mathbf{\Omega}}^{\frac{1}{2}}$ to $\mathbf{l}_k$, the polarimetric leakage errors do not add up perfectly in general. The non-additive nature can be interpreted as a breaking of phase closure [De Zan et al., 2015] due to polarimetric leakage. Conversely, for rank-one interferometric scatterers $\tilde{\mathbf{\Omega}} = \mathbf{a}\mathbf{a}^{\dagger}$, the errors add up.

Acknowledgements

Conflict of interest

FM is a member of the NISAR Science Team.

Author contributions

SZ and FM designed the study; SZ conducted the theoretical and empirical analyses; SZ and FM wrote the manuscript.

Data availability statement

The UAVSAR data are freely available from `https://uavsar.jpl.nasa.gov/`. The IGS TEC products are available from `ftp://gssc.esa.int/gnss/products/ionex/`.

References

E. V. Appleton and G. Builder. The ionosphere as a doubly-refracting medium. *Proceedings of the Physical Society*, 45(2): 208–220, mar 1933. doi: 10.1088/0959-5309/45/2/307.

R. Brcic, A. Parizzi, M. Eineder, R. Bamler, and F. Meyer. Estimation and compensation of ionospheric delay for SAR interferometry. In *2010 IEEE International Geoscience and Remote Sensing Symposium*, pages 2908–2911, July 2010. doi: 10.1109/IGARSS.2010.5652231.

S. R. Cloude and K. P. Papathanassiou. Polarimetric SAR interferometry. *IEEE Transactions on Geoscience and Remote Sensing*, 36(5):1551–1565, Sep. 1998. ISSN 1558-0644. doi: 10.1109/36.718859.

S. R. Cloude and E. Pottier. A review of target decomposition theorems in radar polarimetry. *IEEE Transactions on Geoscience and Remote Sensing*, 34(2):498–518, March 1996. doi: 10.1109/36.485127.

S. R. Cloude, D. G. Goodenough, H. Chen, Y. S. Rao, and W. Hong. Pauli phase calibration in compact polarimetry. *IEEE Journal of Selected Topics in Applied Earth Observations and Remote Sensing*, 11(12):4906–4917, 2018.

Y. Cui, Y. Yamaguchi, H. Yamada, and S. Park. PolInSAR coherence region modeling and inversion: The best normal matrix approximation solution. *IEEE Transactions on Geoscience and Remote Sensing*, 53(2):1048–1060, Feb 2015. doi: 10.1109/TGRS.2014.2332553.

F. De Zan, M. Zonno, and P. Lopez-Dekker. Phase inconsistencies and multiple scattering in SAR interferometry. *IEEE Transactions on Geoscience and Remote Sensing*, 53(12):6608 – 6616, December 2015.

A. G. Fore, B. D. Chapman, B. P. Hawkins, S. Hensley, C. E. Jones, T. R. Michel, and R. J. Muellerschoen. UAVSAR polarimetric calibration. *IEEE Transactions on Geoscience and Remote Sensing*, 53(6):3481–3491, June 2015. ISSN 0196-2892. doi: 10.1109/TGRS.2014.2377637.

A. Freeman and S. S. Saatchi. On the detection of Faraday rotation in linearly polarized L-band SAR backscatter signatures. *IEEE Transactions on Geoscience and Remote Sensing*, 42(8):1607–1616, Aug 2004. doi: 10.1109/TGRS.2004.830163.

G. Gomba, A. Parizzi, F. De Zan, M. Eineder, and R. Bamler. Toward operational compensation of ionospheric effects in SAR interferograms: The split-spectrum method. *IEEE Transactions on Geoscience and Remote Sensing*, 54(3):1446–1461, March 2016. doi: 10.1109/TGRS.2015.2481079.

G. Hartmann and R. Leitinger. Range errors due to ionospheric and tropospheric effects for signal frequencies above 100 MHz. *Bulletin géodésique*, 58:109–136, 1984. doi: 10.1007/BF02520897.

M. Hernández-Pajares, J. M. Juan, J. Sanz, R. Orus, A. Garcia-Rigo, J. Feltens, A. Komjathy, S. C. Schaer, and A. Krankowski. The IGS VTEC maps: a reliable source of ionospheric information since 1998. *Journal of Geodesy*, 83:263–275, 2009. doi: 10.1007/s00190-008-0266-1.

J. R. Jokipii and I. Lerche. Faraday rotation, dispersion in pulsar signals, and the turbulent structure of the galaxy. *Astrophysical Journal*, 157(3):1137–1145, 1969.

K. Kellogg, P. Hoffman, S. Standley, S. Shaffer, P. Rosen, W. Edelstein, C. Dunn, C. Baker, P. Barela, Y. Shen, A. M. Guerrero, P. Xaypraseuth, V. R. Sagi, C. V. Sreekantha, N. Harinath, R. Kumar, R. Bhan, and C. V. H. S. Sarma. NASA-ISRO synthetic aperture radar (NISAR) mission. In *2020 IEEE Aerospace Conference*, pages 1–21, 2020. doi: 10.1109/AERO47225.2020.9172638.

J. S. Kim, K. P. Papathanassiou, R. Scheiber, and S. Quegan. Correcting distortion of polarimetric SAR data induced by ionospheric scintillation. *IEEE Transactions on Geoscience and Remote Sensing*, 53(12):6319–6335, Dec 2015. doi: 10.1109/TGRS.2015.2431856.

J. Lee and T. L. Ainsworth. The effect of orientation angle compensation on coherency matrix and polarimetric target decompositions. *IEEE Transactions on Geoscience and Remote Sensing*, 49(1):53–64, Jan 2011. doi: 10.1109/TGRS.2010.2048333.

F. J. Meyer and J. B. Nicoll. Prediction, detection, and correction of Faraday rotation in full-polarimetric L-band SAR data. *IEEE Transactions on Geoscience and Remote Sensing*, 46(10):3076–3086, Oct 2008. doi: 10.1109/TGRS.2008.2003002.

F. D. Murnaghan. On the field of values of a square matrix. *Proceedings of the National Academy of Sciences*, 18:246–248, 1932.

M. Neumann, L. Ferro-Famil, and A. Reigber. Pol-InSAR coherence set theory and application. In *6th European Conference on Synthetic Aperture Radar*, 2006.

R. Z. Schneider and K. Papathanassiou. Pol-dinSAR: polarimetric SAR differential interferometry using coherent scatterers. In *2007 IEEE International Geoscience and Remote Sensing Symposium*, pages 196–199, July 2007. doi: 10.1109/IGARSS.2007.4422763.

P. A. Wright, S. Quegan, N. S. Wheadon, and C. D. Hall. Faraday rotation effects on L-band spaceborne SAR data. *IEEE Transactions on Geoscience and Remote Sensing*, 41(12):2735–2744, Dec 2003. doi: 10.1109/TGRS.2003.815399.

S. Zwieback and I. Hajnsek. Statistical tests for symmetries in polarimetric scattering coherency matrices. *IEEE Geoscience and Remote Sensing Letters*, 11(1):308–312, Jan 2014. doi: 10.1109/LGRS.2013.2257160.

S. Zwieback and I. Hajnsek. Influence of vegetation growth on the polarimetric DInSAR phase diversity – implications for deformation studies. *IEEE Trans. Geosc. Remote Sens.*, 54(5):3070–3082, 2016.

S. Zwieback, X. Liu, S. Antonova, B. Heim, A. Bartsch, J. Boike, and I. Hajnsek. A statistical test of phase closure to detect influences on DInSAR deformation estimates besides displacements and decorrelation noise: Two case studies in high-latitude regions. *IEEE Transactions on Geoscience and Remote Sensing*, 54(9):5588–5601, Sept 2016. ISSN 0196-2892. doi: 10.1109/TGRS.2016.2569435.